ELSEVIER

Deep-Sea Research II 52 (2005) 3227–3244

DEEP-SEA RESEARCH
PART II

www.elsevier.com/locate/dsr2

Evaluation of shelf–basin interaction in the western Arctic by use of short-lived radium isotopes: The importance of mesoscale processes

David Kadko[a,*], Robin Muench[b]

[a]*University of Miami, RSMAS/MAC, 4600 Rickenbacker Causeway, Miami, FL 33140, USA*
[b]*Earth and Space Research, 1910 Fairview Avenue East, Suite 210, Seattle, WA 98102, USA*

Received 1 May 2004; accepted 15 September 2005

Abstract

Shelf–basin exchange in the western Arctic was evaluated by use of water-column analyses of $^{228}Ra/^{226}Ra$ ratios and the first measurements of the short-lived ^{224}Ra ($T_{1/2} = 3.64$ d) in the Arctic. During the 2002 shelf–basin interaction (SBI) program, excess ^{224}Ra was detected over the shelf but was not found seaward of the shelf-break. Similarly, the $^{228}Ra/^{226}Ra$ ratio dropped rapidly from the shelf across the shelf-break. Consequently, the model age gradient (elapsed time since shelf residence) northward across the Chukchi Shelf increased from 1–5 years nearshore to approximately 14 years in surface waters sampled off shelf at the southern margin of the Beaufort Gyre. This steep gradient is consistent with very slow exchange between the Chukchi Shelf and the Beaufort Gyre, whereby Bering Strait inflow is constrained by the Earth's rotation to follow local isobaths and does not easily move into deeper water. The strong dynamic control inhibiting water that enters the system through Bering Strait from flowing north across isobaths also would lead to a long recirculation time of river water emptied into the Beaufort Gyre. Possible mechanisms that can generate cross-shelf currents that break the topographic constraint to follow isobaths, and thereby transport water (and associated properties) off the shelves include wind-induced upwelling/downwelling, meandering jets, and eddies. Evidence of such a process was found during the ICEX project in the Beaufort Sea in April 2003 when excess ^{224}Ra was measured over 200 km from any shelf source. This required an NE offshore flow of $\sim 40\,cm\,s^{-1}$ assuming that the source water derives from the mouth of Barrow Canyon. A weak northeastward flow was measured using an LADCP within the upper 300 m of the ocean, but was of lower speed than required by the $^{224}Ra_{xs}$ at the time of the ICEX occupation.

Keywords: Arctic Ocean; Radium isotopes; Arctic Shelf; Beaufort Sea; Tracer

1. Introduction

The largely landlocked Arctic Ocean receives input from the Pacific and Atlantic Oceans and from rivers draining the surrounding continents. These inflows provide salt, heat, nutrients, sediment and organisms to the central basin. With the

*Corresponding author. Tel.: +1 305 421 4721; fax: +1 305 421 4689.
E-mail addresses: dkadko@rsmas.miami.edu (D. Kadko), rmuench@esr.org (R. Muench).

0967-0645/$ - see front matter © 2005 Elsevier Ltd. All rights reserved.
doi:10.1016/j.dsr2.2005.10.008

exception of a portion of the Atlantic contribution, they must cross continental shelves where they are modified by benthic, water column, air/sea and sea/ice interactions. The shelves occupy ~35% of the Arctic Ocean's area, and the ratio of shelf to overall basin area is high in comparison to other oceans. The interior Arctic Ocean consequently is strongly influenced by processes occurring on its continental shelves. The modified shelf waters feed the polar surface layer (PSL) and/or ventilate the subsurface layers of the interior basin (Aagaard et al., 1981; Wallace et al., 1987; Melling and Moore, 1995; Schauer et al., 1997), and products of biogeochemical interactions within the shelf environment are transferred into surface and subsurface layers of the Arctic Ocean (Anderson, 1995).

Field observations from the western Arctic suggest that shelf-derived carbon and nutrients are transported to the central Canada Basin (Sambrotto, 1996; Cooper et al., 1997; Walsh et al., 1989, 1997). However, the fate of recently sequestered carbon produced on the shelves depends in part on the nature of shelf–basin interactions and remains poorly known (e.g. Hansell et al., 2004). Recent studies indicate increased anthropogenic contaminant levels, introduced via the shelves from river outflow (e.g. Arctic Monitoring and Assessment Programme (AMAP), 1997), but assessment of this impact likewise depends on knowledge of the exchange rate between the Arctic shelves and the interior basin. To assess better the cross-shelf exchange in this region, the western Arctic Shelf–Basin Interaction (SBI) program was undertaken. This project addresses physical and biological processes within the shelf/slope of the Chukchi and Beaufort seas, with a topical focus on exchange and interaction between Arctic shelves and the basin. Results presented in this paper are a contribution to the SBI program.

We apply here two isotopic tracer techniques to investigate the rate of exchange between the Arctic shelves and interior. With one technique, exchange is evaluated through the first Arctic measurements of the short-lived isotope ^{224}Ra ($T_{1/2} = 3.64$ d). Radium-224, generated in shelf sediment by decay of its parent ^{228}Th, diffuses into the overlying water. There, the ^{224}Ra (in excess of the parent) is transported to the extent that its decay-time allows, providing a measure of short-timescale transport. The second technique measures the water-column ratio of two other naturally occurring radium isotopes, ^{228}Ra/^{226}Ra. Because ^{228}Ra ($T_{1/2} = 5.77$ year) is derived solely through input from shelf sediments, it is an unambiguous marker of water that has been in contact with shelves. Its relative distribution in shelf and basin water is therefore useful for assessing the degree of shelf–basin interaction. Measurements and results reported here are from the spring 2002 SBI field program and from an ice camp (ICEX03) deployed in the Beaufort Sea during spring 2003 (Fig. 1). During the latter exercise, tracer measurements were augmented by lowered acoustic Doppler current profiling (LADCP) to investigate transport processes.

2. Background

2.1. Shelf–basin transport in the western Arctic

Physical reasoning dictates that inflow from Bering Strait to the Arctic Ocean is constrained by the earth's rotation to follow local isobaths, inhibiting cross-shelf transport. Resulting strong along-isobath currents would then be associated with sharp lateral velocity and property gradients across the shelf break and upper slope. However, several processes can potentially transport water and dissolved materials *across* the Arctic shelf and slope. These processes include dense water convection (manifested as downslope plumes), wind-induced shelf break upwelling/downwelling, and frontal instabilities near the shelf break (manifested as eddies and meandering jets). For example, eddies can result from instabilities of the Alaskan Coastal Current where it rounds Point Barrow (D'Asaro, 1988a, b) or from dynamic instabilities accompanying winter brine rejection in coastal areas (Chapman and Gawarkiewicz, 1995; Gawarkiewicz and Chapman, 1995; Chapman, 2000; Gawarkiewicz, 2000). It has been suggested that such features make a significant contribution to the overall flux between the shelf and basins (Manley and Hunkins, 1985; D'Asaro, 1988a, b; Muench et al., 2000).

2.2. Hydrography of the SBI spring 2002 study area

The hydrographic regime within which the SBI spring 2002 samples were collected was described in Hansell et al. (2004). Briefly, for each hydrographic section (Fig. 1), surface water of those stations located over the continental shelf comprised intermediate salinity (32.5–33.5) water of Pacific Ocean origin (via Bering Strait). Present at the northern end of the sections, over the deep Canada Basin,

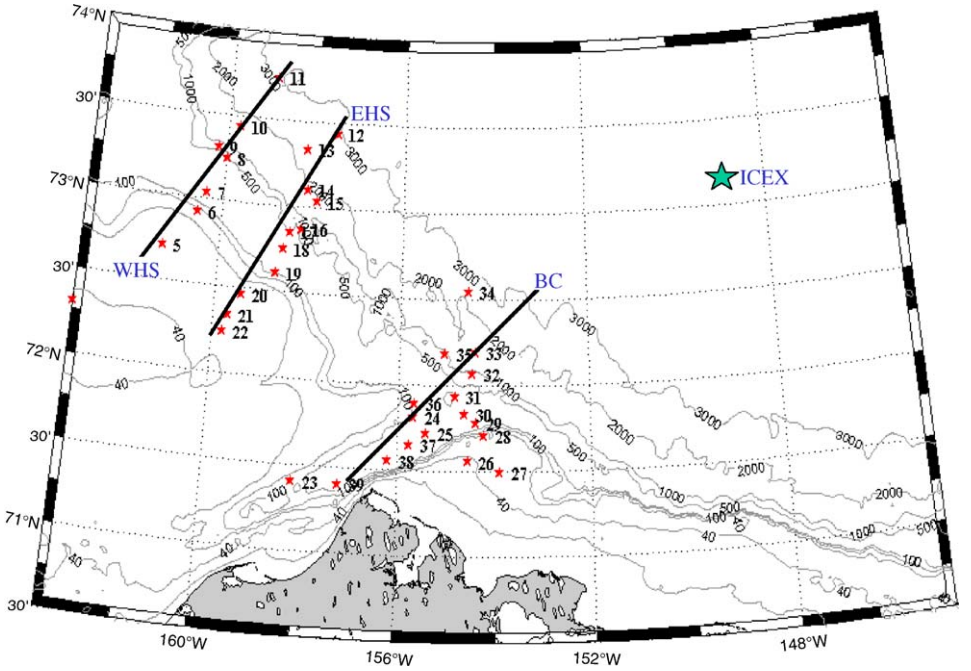

Fig. 1. Location of the SBI spring 2002 transects (WHS = West Hannah Shoal, EHS = East Hannah Shoal, BC = Barrow Canyon) and the 2003 ICEX occupation. Stars indicate station locations.

was the PSL, an ice-covered, relatively low-salinity (<31) water mass that is a mix of riverine and marine waters (e.g. Macdonald et al., 1999). Mixing between the shelf and offshore PSL end-members is shown in surface-water salinity and $\delta\ ^{18}O$ profiles across the shelf break (Fig. 2 middle panels). Note the offshore increase in riverine influence here (lower salinity and $\delta\ ^{18}O$) is unlike that normally found at lower latitudes, where fresher waters are on the shelf. This unusual distribution results from the inflow of Pacific water to the shelf through Bering Strait, and the introduction of largely Mackenzie River water to the offshore PSL east of the study region.

The Pacific Ocean is the primary source of marine water to the PSL and upper halocline water in the western Arctic Ocean, and the Mackenzie and Lena rivers are the largest sources of freshwater (Anderson, 2002). A third end-member in this regime, underlying the Pacific-influenced water, is lower halocline water (~150–220 m depth, core-layer salinity of 34.3) of Atlantic Ocean origin.

2.3. Radium tracers

2.3.1. $^{228}Ra/\ ^{226}Ra$

We utilized two radium isotopic techniques to trace the shelf-water interaction with, and transport to, the central basin. In one, we measured the ratio of two isotopes of radium, ^{228}Ra ($T_{1/2} = 5.77$ year) and ^{226}Ra ($T_{1/2} = 1620$ year) in the water column along transects from the shelf into the basin. Radium is derived from the decay of thorium in the sediments. Radium-228 is produced from the decay of ^{232}Th, and ^{226}Ra from the decay of ^{230}Th. Because radium is mobile in sediment pore water, a fraction of the radium produced there diffuses into the overlying water. Therefore, Ra isotope enrichment occurs in marine waters when they contact sediment, and waters crossing shelves will pick up radium diffused from the underlying sediment. The nearshore $^{228}Ra/\ ^{226}Ra$ ratio will be high because newly injected ^{228}Ra will not have decayed to a great extent. However, because of the relatively short half-life of ^{228}Ra (5.77 year), as the water is transported offshore the $^{228}Ra/\ ^{226}Ra$ ratio will decrease because of radioactive decay and mixing with open ocean water containing little ^{228}Ra (radioactive loss of the long-lived ^{226}Ra over the relevant timescales is negligible). Other tracers of surface water change by evaporation, precipitation and biological activity. The $^{228}Ra/\ ^{226}Ra$ ratio changes, in the absence of additional radium input, only through radioactive decay and mixing with ambient basin waters. This will be the case where shelf water moves offshore

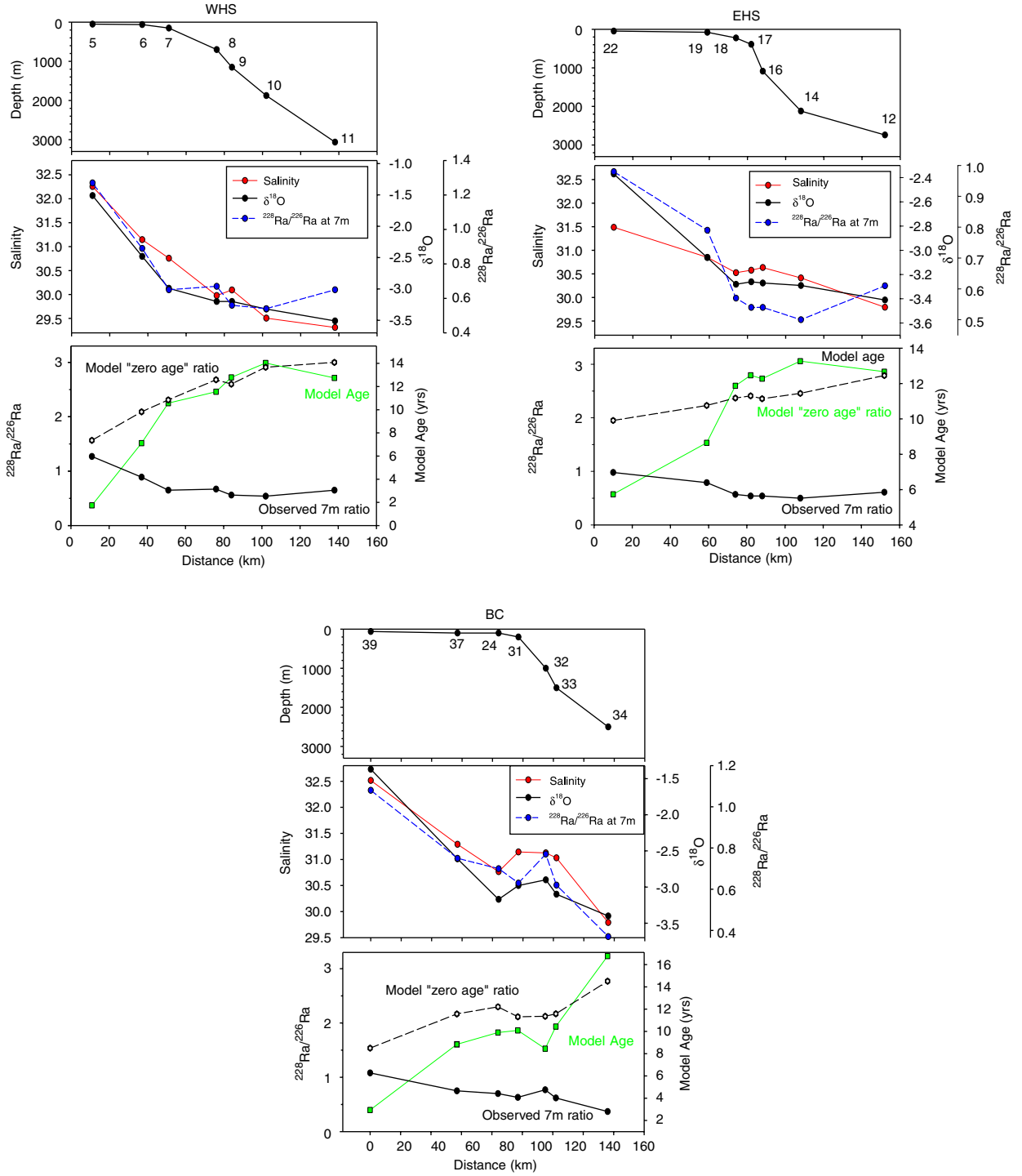

Fig. 2. Horizontal surface property profiles (7 m) for the three transects of the SBI spring 2002 cruise (WHS, EHS, BC). For each transect: top panel: water depth. The station numbers are indicated. Km 0 is defined as the 50-m isobath. Middle panel: Salinity, δ ^{18}O and observed ^{228}Ra/ ^{226}Ra. Note the offshore decrease in salinity and δ ^{18}O indicating the presence of a riverine component in the offshore PSL. Bottom panel: observed ^{228}Ra/ ^{226}Ra; model ^{228}Ra/ ^{226}Ra ratio based on salinity (R_0); model age based on the ratio of observed to modeled ^{228}Ra/ ^{226}Ra.

away from sediment influence. This tracer pair therefore provides a sensitive indicator of shelf water in the ocean and, because of the known decay rate, allows estimation of the rate of shelf–basin exchange. Rutgers van der Loeff et al. (1995) presented ^{228}Ra data from the eastern Arctic Ocean along a section from the Barents Shelf to the Canadian Basin, showing the strong shelf characteristics (high ^{228}Ra/ ^{226}Ra) of surface waters advected in the Transpolar Drift (TPD) towards Fram Strait. There, high ^{228}Ra/ ^{226}Ra ratios indicate rapid transport of surface water from the Eurasian and Siberian shelves into the central Arctic Ocean. In contrast, ^{228}Ra/ ^{226}Ra ratios in the surface Beaufort Gyre at Ice Station T3 are very low (Kaufman et al., 1973), suggesting a long recirculation time of river water within that circulation.

Here, we adopt the model of the ^{228}Ra/ ^{226}Ra vs. salinity relationship that describes aging of water advecting from the eastern Arctic shelves (Rutgers van der Loeff et al., 1995), and as recently applied to the western Beaufort Gyre (Hansell et al., 2004). Fig. 3, (left panel) illustrates the case of a simple, two-end-member situation with an expected mixing trend (line "a"), *with zero aging*, between a typical, low-salinity, low-δ^{18}O, high ^{228}Ra/ ^{226}Ra "young" shelf end-member with a high-salinity, high-δ ^{18}O, low ^{228}Ra/ ^{226}Ra ocean end-member. This trend defines an expected ^{228}Ra/ ^{226}Ra ratio for a given salinity under the circumstances of *rapid* mixing with respect to the half-life of ^{228}Ra. For example, Rutgers van der Loeff et al. (1995) utilized the trend defined by data in the TPD, indicating rapid export of those waters from the eastern Arctic shelf to the Arctic Ocean interior. Observed ^{228}Ra/ ^{226}Ra ratios lower than expected (for zero age mixing alone) for a given salinity (Fig. 3, left panel) represent aging of that water mass and can be used to compute the elapsed time since contact with shelf sediments. The low-salinity, low-δ ^{18}O shelf water indicates significant influence from river outflow.

The model is similar given a third end-member and the unusual hydrography of the western Arctic observed during the SBI 2002 cruise (see Section 2.2). Here, the third end-member was PSL water of low salinity and low δ ^{18}O that was observed offshore, over the deep basin. Despite the low salinity and low δ ^{18}O indicative of riverine influence, this water had low ^{228}Ra/ ^{226}Ra, suggesting "aging" since residence on the shelf (Hansell et al., 2004). In this three end-member model (Fig. 3, right panel) the measurements will fall between the conservative mixing lines defined by the end-members. Again, ^{228}Ra/ ^{226}Ra ratios lower than the expected zero age mixing trend represent aging of that water mass and the age of the mixture can be derived.

Elapsed time-since-residence on the shelf (T) is derived from the simple radioactive decay equation:

$$T = -\ln[R/R_0]\lambda, \quad (1)$$

where λ is the decay constant of ^{228}Ra (year^{-1}), R the observed ^{228}Ra/ ^{226}Ra ratio, and R_0 is the ^{228}Ra/ ^{226}Ra ratio expected for a given salinity with no aging (from line "a", derived empirically

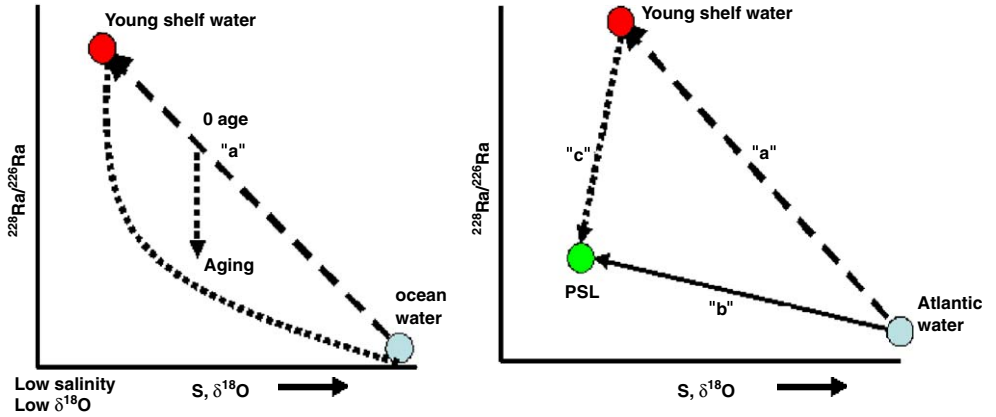

Fig. 3. Model of the ^{228}Ra/ ^{226}Ra ratio over the shelf-break. Left: two end-member case. The dashed arrow (line "a") indicates rapid mixing (zero age time-since-shelf residence) between a typical shelf (low salinity, low δ ^{18}O) and the ocean basin. As a parcel of water moves offshore, the ^{228}Ra/ ^{226}Ra ratio will decrease with aging (dotted line). Right: three end-member case, with the addition of aged, river-influenced water offshore (in the PSL) as was observed during SBI 2002 in the western Arctic (see text).

from the data). Rutgers van der Loeff et al. (1995) defined the $^{228}Ra/^{226}Ra$-salinity trend of the TPD as the zero age (R_0) trend in their study of the eastern Arctic, but they noted the trend is not precisely a "zero age" trend as uncertainty precludes dating to better than <3 years. However, for the purpose of that study and for the work here, such uncertainty is small relative to the large range in $^{228}Ra/^{226}Ra$ observed across the Arctic. Also, while ratios do not necessarily mix linearly, the range in ^{226}Ra activity in the upper water is small compared to that of ^{228}Ra, such that aging effects are reasonably represented by consideration of the $^{228}Ra/^{226}Ra$ ratio.

2.3.2. ^{224}Ra

We also utilize here the first measurements in the Arctic Ocean of the short-lived isotope ^{224}Ra ($T_{1/2} = 3.64$ d). The ^{224}Ra is produced from decay of ^{228}Th, which is itself produced by ^{228}Ra. The ^{228}Th is concentrated in sediments and, due to its high particle reactivity, has only a small activity in coastal waters. In such cases the seawater activity ratio of $^{228}Th/^{228}Ra$ is typically <0.05 (Kaufman et al., 1981), so nearshore background ^{224}Ra from seawater ^{228}Th will be small compared to that diffusing from the shelf sediments. The ^{224}Ra activity above the background ^{228}Th activity is defined as excess ^{224}Ra ($^{224}Ra_{xs} = {}^{224}Ra_{total} - {}^{228}Th$), and will decay to the ^{228}Th background once the water parcel is removed from sediment contact. The short half-life of ^{224}Ra allows its use for evaluation of rapid cross-shelf transport processes.

3. Methods

Measurements and results reported here are from the SBI process cruise in spring 2002 and from an ice-camp occupation (ICEX 03) in the Beaufort Sea during spring 2003 (Fig. 1).

3.1. Radium analysis

During the 2002 SBI cruise, 220 L samples for radium analysis were taken from ~7 m depth through the hull-mounted intake line of the research icebreaker USCGC *Healy*. Water was collected for deeper samples (to 250 m) by triggering 30 L rosette-mounted bottles at the desired depth to obtain samples of 160–220 L. During the 2003 ice-camp occupation, water samples were pumped with an electric centrifugal pump through a garden hose suspended through a 1-m diameter hole that had been melted through the ice. Samples were collected in 50-gallon plastic drums that were then slowly drained with electric pumps (~1 L min^{-1}) through plastic tubes packed with manganese-coated acrylic fibers. It has been shown that these fibers adsorb radium isotopes efficiently and without fractionation (Moore et al., 1985). After drainage, each fiber-filled tube was placed in a stripping line, and ^{224}Ra was determined by counting its daughter ^{220}Rn ($T_{1/2} = 55.6$ s). Within a closed circulation loop, ^{220}Rn was stripped by helium directly into a ZnS-coated, scintillation cell/photomultiplier delayed coincidence counting system (Moore and Arnold, 1996). The efficiency of the system is determined by a ^{228}Th (parent of ^{224}Ra) standard. This procedure is replicated for most samples over a period of several weeks to determine the ^{228}Th activity of the sample. For some samples in 2002, the second count was not performed until many weeks after the cruise, such that the ^{228}Th activity had to be corrected for ingrowth from its ^{228}Ra parent. After ^{224}Ra counting, the acrylic fibers were sealed in plastic petri dishes where, on land, ^{228}Ra and ^{226}Ra activities were determined by measuring the activity of the radium daughters by gamma ray spectrometry (Michel et al., 1981). The counting system is calibrated with known radioactive sources using a geometry that matches that of the fiber samples. Our laboratory utilizes two low-background, high-efficiency germanium detector systems.

3.2. LADCP and ice-camp CTD observations

From 3 to 12 April 2003, a sequence of 23 vertical profiles of the horizontal upper-ocean currents was measured from the ICEX ice camp using a LADCP. The current profiler, an internally recording, 600 kHz RDI unit that consisted of synchronized upward and downward looking acoustic heads, was mounted on the same frame as a SeaBird SBE 19 SeaCat self-contained conductivity, temperature and depth profiler (CTD).

The current profiles started about 2 m below the surface and extended to depths varying from 500 to 1000 m. Two or three profiles were obtained each day. The data were processed with the widely used software suite developed by Martin Visbeck (LDEO, Columbia University) and described on a website maintained at http://www.ldeo.columbia.

edu/~visbeck/ladcp/. The processed data returned a nominal velocity error, over all but the uppermost and lowermost 50 m of each profile, of ~1–2 cm s^{-1}. Absolute currents were derived from the observed relative currents using ice drift speeds derived from one of several available GPS systems. Comparisons among two different sets of GPS observations, coupled with the fact that sea ice does not undergo significant drift change over the maximum timescale (~45 min) of a single LADCP cast, suggest that ice-drift velocities were accurate to within the LADCP accuracy.

The CTD returned T, C and P data that were later used to compute S and density. No in situ calibrations were obtained for the CTD; however, calibration at the SeaBird calibration facility directly prior to and following the ice camp showed no significant shift in the calibrations, and all calibrations were well within instrument specifications (better than 0.005 in T and S).

4. Results and discussion

4.1. SBI spring 2002

Radium analyses for the SBI spring 2002 samples are presented in Table 1. The surface salinities, $\delta^{18}O$ and $^{228}Ra/^{226}Ra$ ratios measured on the three spring 2002 transects are shown in Fig. 2 (middle panels). All transects show a decrease in salinity and $\delta^{18}O$ offshore, consistent with the presence of river water seaward of the shelf break. Of note is the sharp offshore decrease in $^{228}Ra/^{226}Ra$. While not surprising that the ratio is lower away from the sediment source region, the presence of low $^{228}Ra/^{226}Ra$ within the offshore low-salinity and low-$\delta^{18}O$ water indicates that the offshore freshwater is recirculated, aged river water within the Beaufort Gyre. The gradient in $^{228}Ra/^{226}Ra$ (and by implication, elapsed time-since-shelf interaction) across the shelf break is striking. In Fig. 4, the $^{228}Ra/^{226}Ra$ ratios from all depths are plotted against salinity and $\delta^{18}O$. The three end-members are indicated.

A model age differential across the shelf break can be derived using the $^{228}Ra/^{226}Ra$–S relationships of the study site as discussed in Section 2.3.1. Fig. 4A shows that $^{228}Ra/^{226}Ra$ ratios measured from all depths fall between line "a" and the line delineated by Beaufort Gyre data at Ice Station T3. The former describes rapid mixing (zero age), thus serving as R_0 (Eq. (1)) for this area. It is defined by nearshore samples (those from stations shallower than the 500 m isobath, excluding the anomalous offshore data from Barrow Canyon shown in the figure). The T3 line defines older, recirculated water within the Beaufort Gyre (Rutgers van der Loeff et al., 1995).

It is interesting to note that the TPD radium data describing rapid transport (zero age) off the eastern Arctic shelves defines a $^{228}Ra/^{226}Ra$-salinity relationship similar to the Beaufort data (line "a") presented here (Fig. 4A). It has previously been suggested that the zero age western Arctic water manifests a lower $^{228}Ra/^{226}Ra$-salinity slope than the TPD trend (Smith et al., 2003; Rutgers van der Loeff et al., 2003). However, this suggestion was based on a limited data set (Fig. 3 in Smith et al., 2003) in which no clear trend is apparent.

In Fig. 2 (bottom panels) the $^{228}Ra/^{226}Ra$ ratios expected along the section, where there was no radioactive decay (zero-age water), are modeled as a function of salinity, where $R_0 = -0.486S + 17.25$. Again, this function is derived from the rapid mixing line "a". These are compared to the *observed* $^{228}Ra/^{226}Ra$ ratios, and the model age (elapsed time-since-shelf residence) is calculated from the ratio of [(observed $^{228}Ra/^{226}Ra$)/R_0] using Eq. (1). Calculated age increased steeply, from <5 years over the shelf to ~14 years for surface waters sampled at the southern edge of the Beaufort Gyre. This gradient is consistent with very slow exchange between this section of the Arctic shelf and the basin interior, suggesting that the dynamic constraint limiting cross-isobath flow and the consequent eastward flowing boundary current present a hindrance to cross-shelf exchange. This would lead to a long recirculation time for river water emptied into the Beaufort Gyre (Hansell et al., 2004). Not surprisingly, the $^{224}Ra_{xs}$ data show a similar result. In particular, for sections EHS and WHS, $^{224}Ra_{xs}$ was found only within ~60 km of the coast (Fig. 5). Note that higher $^{224}Ra_{xs}$ was observed at depth because of the bottom source and short ^{224}Ra half-life. These data indicate that rapid offshore transport was not occurring along these sections during the spring 2002 cruise. For section BC, there is indication of $^{224}Ra_{xs}$ farther offshore, which is also reflected in the $^{228}Ra/^{226}Ra$ ratios for several samples.

4.2. ICEX spring 2003

Radium analyses for ICEX spring 2003 are presented in Table 2. Vertical profiles of T, S, $^{224}Ra_{xs}$

Table 1
Radiochemical data from SBI spring 2002

Sample	Depth (m)	Salinity	^{224}Ra (dpm 100 l^{-1})	^{228}Th (dpm 100 l^{-1})	^{224}Ra$_{xs}$ (dpm 100 l^{-1})	^{226}Ra (dpm 100 l^{-1})	^{228}Ra (dpm 100 l^{-1})	$\frac{^{228}\text{Ra}}{^{226}\text{Ra}}$
HV[a]								
0–1	5	32.8613	1.65±0.10	0.26±0.09	1.39±0.14	14.07±0.87	6.51±0.49	0.46±0.05
0–2	41	33.073	1.61±0.13	bd	1.61±0.22	8.04±0.38	4.77±0.24	0.59±0.04
1–1	5	33.0851	1.36±0.07	0.19±0.06	1.17±0.10	5.79±0.64	4.15±0.56	0.72±0.12
1–2	40	33.0977	0.89±0.10	0.15±0.09	0.74±0.13	3.84±0.09	2.49±0.06	0.65±0.02
2–1	5	33.0318	0.66±0.17	bd	0.66±0.62	5.79±0.40	7.08±1.29	1.22±0.24
2–2	40	33.0703	1.4±0.2	bd	1.4±0.59	14.83±1.72	12.42±1.20	0.84±0.13
3–1	5	33.5463	1.13±0.08	0.015±0.13	1.115±0.06	4.99±0.15	5.45±0.73	1.09±0.15
3–2	39	33.6316	0.94±0.07	0.36±0.11	0.58±0.13	6.00±0.49	5.31±0.95	0.88±0.17
WHS								
5–1	7	32.2715	0.6±0.05	0.41±0.09	0.19±0.10	5.79±0.21	7.37±0.72	1.27±0.13
5–2	45	32.8007	3.4±0.15	bd	3.4±0.23	7.42±0.46	8.95±0.35	1.21±0.09
6–1	7	31.1942	1.29±0.07	1.17±0.20	0.12±0.22	8.63±0.56	7.69±0.51	0.89±0.08
6–2	55	32.7967	2.48±0.10	0.34±0.10	2.14±0.14	6.61±0.55	7.60±0.94	1.15±0.17
7–1	7	30.7329	1±0.1	1.2±.1	−0.2±0.1	7.01±0.42	4.55±0.75	0.65±0.11
7–2	96	32.5771	1.00±0.09	bd	0±0.2	5.91±0.42	7.41±0.32	1.25±0.10
7–3	144	34.542	2.82±0.08	bd	2.82±0.33	10.66±1.36	5.43±0.59	0.51±0.09
8–1	7	29.9805	2.70±0.12	0.26±0.09	0.77±0.37	8.26±0.54	5.55±0.60	0.67±0.08
8–2	250	34.7	1.2±0.05	bd	0.26±0.5	4.85±0.63	1.00±0.82	0.21±0.17
8–3	50	31.789	1.05±0.15	1.1±1.2	−0.05±1.1	16.05±2.53	8.98±1.96	0.56±0.15
8–4	140	33.2641	1.4±0.4	1.6±0.3	−0.2±0.5	6.02±0.74	3.69±0.64	0.61±0.13
9–1	7	30.1412	1.74±0.10	1.79±0.6	−0.05±0.56	5.55±0.67	3.12±1.18	0.56±0.22
9–2	60	34.6448	1.37±0.11	1.53±0.14	−0.16±0.18	5.21±0.39	3.90±0.72	0.75±0.15
9–3	150	33.4864	1.4±0.15	0.65±0.77	0.75±0.78	7.90±0.41	5.70±1.18	0.72±0.15
9–4	200	34.3536	1.50±0.09	0.5±0.5	1±0.5	4.74±0.32	1.51±0.72	0.32±0.15
10–1	7	29.5011	1.61±0.09	1.60±0.16	0.01±0.19	5.64±0.54	3.05±0.78	0.54±0.15
10–2	200	34.2706	1.1±0.1	1.3±0.6	−0.2±0.6	5.99±0.63	4.37±0.94	0.73±0.18
10–3	150	33.2879	2.09±0.4	1.27±0.13	0.82±0.18	5.44±0.71	1.26±0.11	0.23±0.04
10–4	50	31.7347	1.94±0.17	1.46±0.12	0.48 ±0.21	6.77±0.49	4.41±0.07	0.65±0.05
10–5	100	32.6396	1.43±0.09	1.64±0.14	−0.21±0.17	5.56±0.48	4.29±1.19	0.77±0.22
11–1	7	29.3064	1.39±0.11	1.67±0.8	−0.28±0.14	4.94±0.26	3.23±0.05	0.65±0.04
11–2	50	31.6057	1.60±0.09	1.53±0.11	0.07±0.14	8.07±0.55	5.19±2.04	0.64±0.26
11–3	150	33.2433	1.4±0.08	2.0±0.1	−0.6±0.13	6.58±0.53	4.60±0.53	0.70±0.10
11–4	100	32.5067	1.9±0.13	bd	1.9 ±1.9	23.15±4.39	13.23±3.15	0.57±0.17
EHS								
12–1	7	29.7546	1.71±0.09	1.67 ±0.11	0.04 ±0.15	5.71±0.40	3.46±0.37	0.61±0.08
12–2	45	31.507	1.35±0.09	1.33 ±0.09	0.02 ±0.14	5.21±0.34	2.27±0.37	0.44±0.08
12–3	220	34.34	1.09±0.09	1.48 ±0.10	−0.39±0.14	9.69±2.22	4.09±0.51	0.42±0.11
12–4	150	33.1218	1.92±0.13	1.91±0.12	0.01 ±0.18	9.59±0.59	4.98±0.41	0.52±0.05
14–1	7	30.4383	1.31±0.06	1.49±0.06	−0.18±0.09	6.785±0.25	3.36±0.14	0.50±0.03
14–2	150	33.394	1.52±0.30	1.04±0.06	0.48±0.31	31.60±8.15	10.14±0.66	0.32±0.09
14–3	45	31.6377	1.27±0.06	1.18±0.08	0.09±0.11	14.10±2.77	9.34±0.58	0.66±0.14
14–4	250	34.5505	1±0.07	0.1±0.8	0.9±0.8	9.15±1.40	3.38±1.29	0.37±0.15
14–5	200	34.1237	1.22±0.08	bd	1.22±0.9	30.10±8.44	10.52±1.51	0.35±0.11
16–1	7	30.6477	1.69±0.07	1.44±0.17	0.25±0.18	7.15±0.91	3.85±0.33	0.54±0.08
16–2	140	33.2047	1.80±0.18	1.32±0.11	0.48±0.21	9.51±0.74	9.84±0.52	1.03±0.10
16–3	80	32.2565	1.6±0.1	2.1±0.1	−0.5±0.1	6.705±0.78	2.68±0.82	0.40±0.13
16–4	250	34.7497	0.8±0.09	0.9±0.08	−0.1±0.1	7.39±1.11	1.65±0.63	0.22±0.09
17–1	7	30.5381	1.74±0.10	1.37±0.13	0.37±0.52	7.72±0.45	4.13±2.31	0.54±0.30
17–2	135	33.1527	1.49±0.10	1.70±0.11	−0.21±0.15	8.33±0.64	4.17±1.59	0.50±0.19
17–3	75	32.1735	1.14±0.13	0.8±0.8	0.34±0.8	11.40±0.64	9.32±1.31	0.82±0.12
17–4	250	34.7753	0.60±0.03	0.53±0.9	0.07±0.9	5.65±0.13	0.68±1.39	0.12±0.25
17–5	205	34.5977	0.87±0.09	0.3±1.2	0.57±1.2	7.27±0.30	1.75±1.66	0.24±0.23
18–1	7	30.62	1.29±0.08	1.28±0.10	0.01±0.12	6.06±0.40	3.44±0.23	0.57±0.05
18–2	215	34.7657	1.66±0.06	0.62±0.11	1.04±0.13	5.16±0.63	2.36±1.55	0.46±0.31

Table 1 (*continued*)

Sample	Depth (m)	Salinity	^{224}Ra (dpm 100 l^{-1})	^{228}Th (dpm 100 l^{-1})	^{224}Ra$_{xs}$ (dpm 100 l^{-1})	^{226}Ra (dpm 100 l^{-1})	^{228}Ra (dpm 100 l^{-1})	$\frac{^{228}\text{Ra}}{^{226}\text{Ra}}$
18–3	110	32.7025	1.05±0.08	0.99±0.05	0.06±0.1	7.24±0.89	6.25±1.55	0.86±0.24
19–1	7	30.9044	0.91±0.05	1.14±0.21	−0.23±0.22	7.31±0.50	5.78±0.39	0.79±0.08
19–2	70	32.5799	2.11±0.08	0.19±0.3	1.92±0.31	9.19±0.10	11.49±0.61	1.25±0.07
22–1	7	31.4811	1.11±0.11	0.44±0.49	0.67±0.5	7.41±0.41	7.29±1.07	0.98±0.15
22–2	41	32.6569	3.10±0.08	0.17±0.24	2.93±0.25	8.72±0.83	11.59±0.48	1.33±0.14
BC								
24–1	7	30.7653	1.42±0.09	0.99±0.11	0.43±0.14	6.29±0.79	4.38±0.20	0.70±0.09
24–2	91	32.7472	2.78±0.12	0.66±0.37	2.12±0.16	11.92±0.97	10.47±0.57	0.88±0.09
24–3	45	31.7442	1.41±0.12	1.02±1.03	0.39±1.04	9.84±0.63	7.53±1.66	0.77±0.18
27–1	7	31.8543	0.69±0.10	0.55±0.66	0.14±0.66	8.72±0.24	9.01±1.44	1.03±0.17
27–2	33	32.7951	0.78±0.06	0.94±0.31	−0.16±0.32	9.41±0.44	7.62±0.64	0.81±0.08
31–1	7	31.1433	1.17±0.08	0.42±0.37	0.75±0.38	7.70±0.47	4.88±0.81	0.63±0.11
31–2	250	34.7107	1.02±0.06	0.08±0.12	0.94±0.14	6.86±0.70	2.54±0.24	0.37±0.05
31–3	200	34.4816	1.48±0.07	0.85±0.92	0.63±0.92	7.98±0.23	4.14±1.48	0.52±0.19
31–4	90	32.791	1.55±0.07	1.75±0.83	−0.20±0.83	9.80±0.23	6.27±1.32	0.64±0.14
32–1	7	31.1259	1.25±0.05	0.23±0.41	1.02±0.42	8.17±0.65	6.28±0.88	0.77±0.12
32–2	175	34.2388	1.28±0.07	0.31±0.46	0.97±0.47	10.32±0.28	7.96±0.71	0.77±0.07
32–3	100	32.8227	0.92±0.07	0.48±0.57	0.44±0.57	11.53±0.41	11.51±0.89	1.00±0.08
32–4	250	34.6387	0.77±0.07	1.11±0.50	−0.34±0.51	6.54±0.44	2.59±0.78	0.40±0.12
32–5	50	31.7817	1.09±0.07	0.69±0.22	0.40±0.24	8.23±1.03	6.61±0.28	0.80±0.11
33–1	7	31.0309	0.95±0.11	0.53±0.53	0.42±0.54	7.04±0.62	4.38±1.16	0.62±0.17
33–2	165	33.7783	0.63±0.15	0.14±0.48	0.49±0.50	7.59±0.16	8.20±0.77	1.08±0.10
33–3	100	32.8795	1.6±0.07	0.88±0.86	0.72±0.86	8.96±0.56	4.18±1.37	0.47±0.16
33–4	250	34.5339	0.49±0.11	0.85±0.36	−0.36±0.38	7.03±0.58	2.76±0.79	0.39±0.12
34–1	7	29.7913	2.52±0.12	1.47±0.34	1.05±0.36	8.33±0.37	3.11±0.73	0.37±0.09
34–2	100	32.7672	1.49±0.07	2.09±0.66	−0.60±0.67	10.11±0.49	6.18±1.05	0.61±0.11
34–3	50	32.0094	1.93±0.16	2.23±0.15	−0.3±0.22	7.58±0.27	3.90±0.21	0.51±0.03
34–4	170	33.6644	1.20±0.12	0.77±0.27	0.43±0.30	8.79±0.69	7.07±0.59	0.80±0.09
37–1	7	31.2907	1.11±0.12	1.08±0.41	0.03±0.43	7.07±0.8	5.26±0.9	0.74±0.15
37–2	50	32.0897	1.19±0.17	1.43±1.03	−0.24±1.04	8.28±0.21	6.31±1.66	0.76±0.20
37–3	80	32.3874	1.06±0.17	1.06±0.76	0±1.22	6.96±0.81	8.23±1.22	1.18±0.22
37–4	150	33.4212	2.37±0.17	0.4±0.6	1.97±0.7	9.99±0.49	10.24±1.04	1.03±0.12
39–1	7	32.5161	0.68±0.05	0.01±0.2	0.67±0.20	6.17±0.25	6.64±0.46	1.08±0.09
39–2	45	32.8993	1.82±0.07	1.02±0.84	0.80±0.84	9.68±0.32	8.14±1.34	0.84±0.14
39–3	100	33.6032	1.17±0.07	0.6±1.2	0.57±1.2	9.15±1.2	9.06±1.90	0.99±0.24

[a]HV station locations: Station 0: 65°00.53′N, 169°03.12′W; Station 1: 67°28.115′N, 168°51.78′W; Station 2: 70°38.35′N, 167°23.60′W; Station 3: 71°52.76′N, 166°05.44′W.

and horizontal currents are shown in Figs. 6A–D for those profiles analyzed for radium isotopes 3–10 April 2003.

The current profiles indicate an east–northeastward upper ocean (0–250 m) flow, with intermittent speed maxima near 100 m, that persisted throughout the 10-day period over which currents were measured from the spring 2003 ice camp (Fig. 7). Current speeds associated with this layer were ~5 cm s^{-1}. This flow was limited to the upper and middle halocline layers, and the intermittent ~100 m speed maximum occupied the middle halocline as defined in the vertical S distribution by an inflection in the profile near 33.1 and 150 m depth (Figs. 6A–D). Comparison with profiles presented in McLaughlin et al. (2004) show the vertical distributions of T and S to be typical for the Beaufort Sea from the Northwind Abyssal Plain nearly to the Canadian Archipelago, corresponding to their "Type II" water mass. Middle halocline water is Pacific origin water, and the associated minimum T reflects intermittent addition of water that has been modified by cooling and salinization through ice formation on the continental shelves to the south (Melling and Moore, 1995).

Within the upper 250 m there is also ^{224}Ra$_{xs}$, with maximum values between 50 and 150 m. The presence of ^{224}Ra$_{xs}$ here, ~200-km offshore,

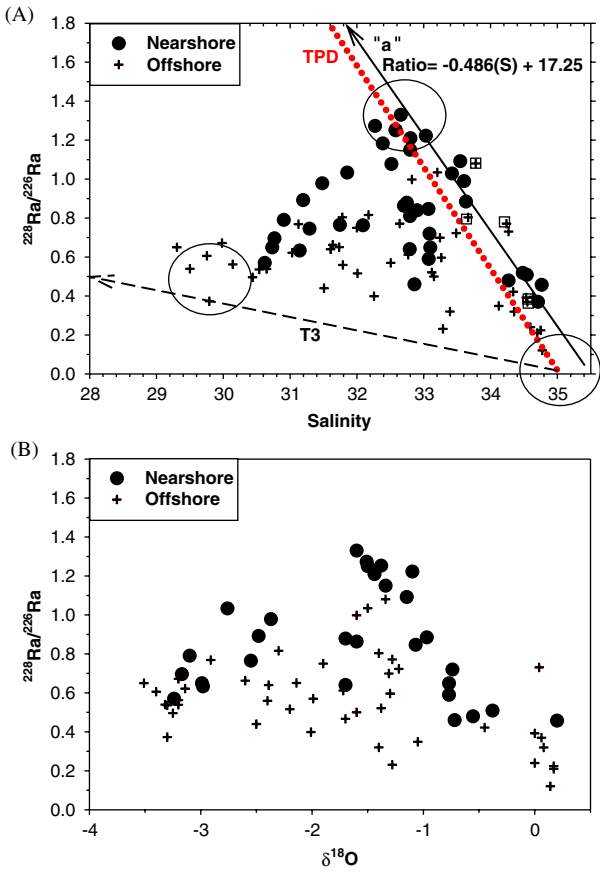

Fig. 4. (A) The $^{228}Ra/^{226}Ra$ ratios from all depths plotted against salinity. The SBI data fall between the ratios defined by the zero-age trend (upper arrow "a") and by the Beaufort Gyre data at Ice Station T3 (lower arrow). Barrow Canyon offshore samples with high $^{228}Ra/^{226}Ra$ (indicated by ⊞) were not used to define the upper trend. The T3 trend represents older, recirculated water within the Beaufort Gyre. End-members described in text are indicated by circles. The zero-age trend of the Transpolar Drift (TPD) trend off the eastern Arctic shelves into the Arctic Basin is shown for comparison. (B) The $^{228}Ra/^{226}Ra$ ratios plotted against $\delta^{18}O$. (The $\delta^{18}O$ data provided by L. Cooper; note: $\delta^{18}O$ not available for all radium samples.)

is noteworthy because its short half-life requires extremely rapid offshore transport. In sharp contrast, the spring 2002 transects (perhaps excepting section BC) to the west showed $^{224}Ra_{xs}$ confined to within 60 km of the coast.

The observation of significant amounts of $^{224}Ra_{xs}$ at ICEX warrants closer inspection. Conceivably, fractionation of ^{224}Ra and ^{228}Th during the analytical procedure (for example, preferential loss of ^{228}Th during filtering) could lead to an apparent $^{224}Ra_{xs}$. However, internal consistency of the data indicates otherwise. For all profiles the $^{224}Ra_{xs}$ tends to 0 at depth, and reproducibly approaches 0 for the deepest samples (two points at 250 m, cast D) of the study. Also, the profiles of April 3 and 6 are similar to each other. Fractionation of ^{228}Th would likely be random and at variance with these observations. In addition, the measured ^{228}Th activities are not small compared to values from the literature (Rutgers van der Loeff et al., 1995) or from the SBI spring transects presented in Table 1. Similar reasoning would tend to preclude natural fractionation in the water column. If ^{228}Th and ^{224}Ra were in equilibrium in the water column, an event capable of scavenging ^{228}Th on a timescale shorter than the decay rate of ^{224}Ra would be required. Scavenging of thorium on this timescale is not reasonable (e.g. Coale and Bruland, 1985).

Another source of $^{224}Ra_{xs}$ could be diffusion from ice-borne sediments (as opposed to sediments from the seafloor). Assuming that ice-borne material and sea-floor sediments have similar isotopic activities, then the relative fluxes of ^{224}Ra between the two sources would depend on the ratio of the dry bulk density of seafloor sediment to that of ice. Although ice rafting of sediment has importance for the Arctic sediment transport budget (Reimnitz et al., 1993) typical dry bulk densities of Arctic ice are several orders of magnitude less than that of seafloor sediments and thus ice input can reasonably be assumed to be negligible.

It is not possible to determine the upstream source of the ICEX feature to ascertain the initial $^{224}Ra_{xs}$ at the source region and thus calculate the speed of offshore transport. Using the ^{224}Ra mean-life (5.25 d), and considering that the nearest shelf region (Barrow Canyon) is approximately 200 km away from the ICEX site, a speed of $\sim 40\,cm\,s^{-1}$ would be required. Following the high values observed early during ICEX, the ^{224}Ra levels subsequently decreased at a rate consistent with natural decay (Fig. 8). While certainly, interannual variability complicates comparison, the core of the ICEX feature at 150 m has T–S characteristics similar to several SBI spring 2002 stations occupied over the shelf break. There is also consistency in the $^{228}Ra/^{226}Ra$ ratios of the shelf-break stations with those within the ICEX feature (0.49–0.81; Fig. 7). This suggests that water with shelf-break characteristics must have advected over shelf sediments during a period of several days to accumulate the shorter-lived ^{224}Ra.

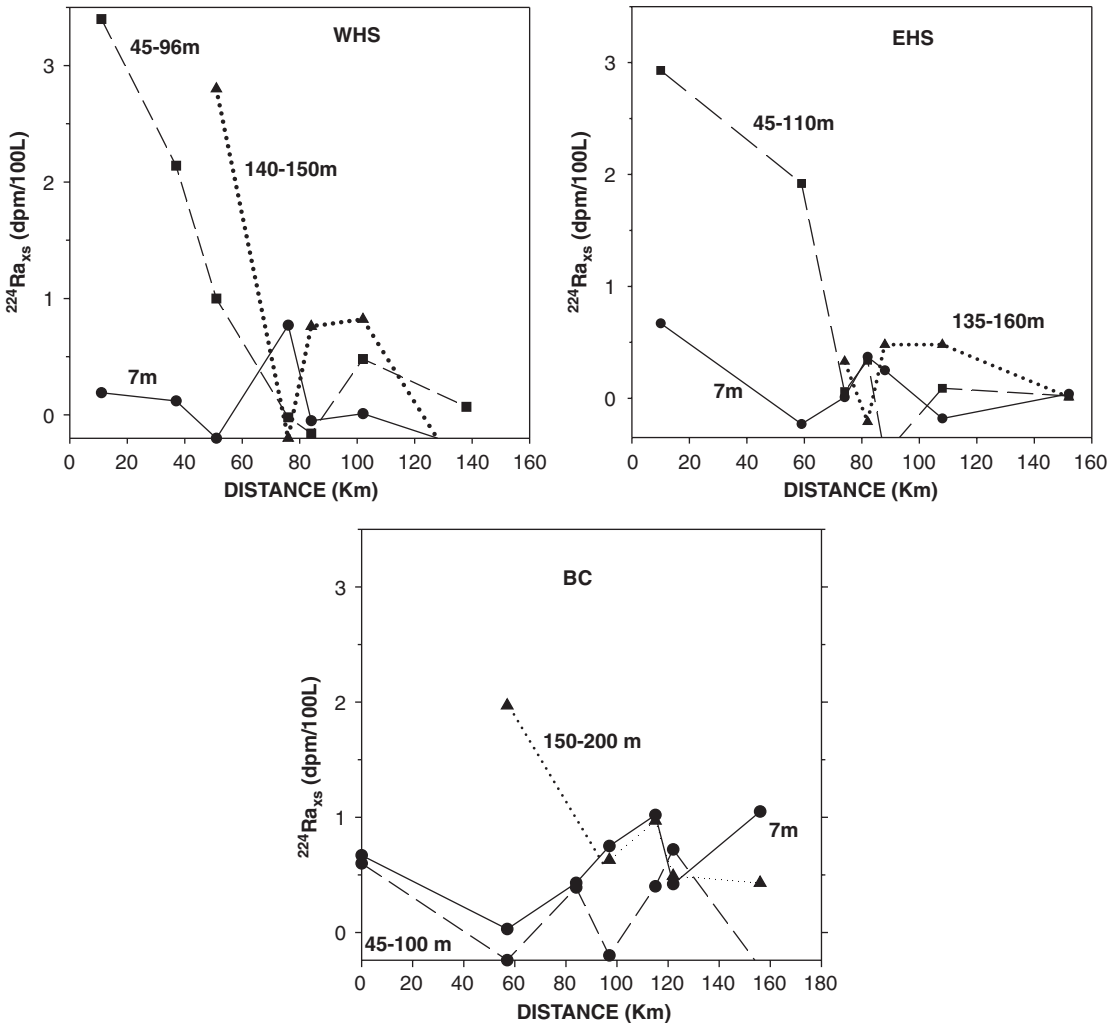

Fig. 5. $^{224}Ra_{xs}$ profiles for the three SBI spring 2002 transects. Km 0 is defined as the 50-m isobath.

The $^{228}Ra/^{226}Ra$ ratios would not be affected within this timescale.

While the 0–250 m waters appear to have their origins in Pacific water that has been modified while traversing the shallow shelves to the south, physical mechanisms through which the observed tracer-rich water might have been transported from the nearest shelf region with the required rapidity are uncertain. The nearest such region is ~200 km distant from the ice station position (Fig. 1). It seems unlikely that our short-term observations of a $5\,cm\,s^{-1}$ east–northeast flow in the cold halocline layer represent a long-term mean current because this is counter to westward geostrophic flow that is normally assumed to be associated with the Beaufort Gyre (McLaughlin et al., 2004). This current is in the proper direction to transport tracers from the shelf; however, the speed is an order of magnitude too low to have been solely responsible for transport of the very short-lived ^{224}Ra isotope over the necessary distance. Other mechanisms need to be invoked in order to explain presence of the tracers at the ice station site.

Recent modeling work by Winsor and Chapman (2004) suggests that northward-flowing Pacific water fans out over the Chukchi Shelf and has little tendency toward forming distinct branches. Previous field-based work has shown, however, that Herald and Barrow canyons—particularly the latter—and the Alaska Coastal Current, can play major roles in channeling Pacific origin water into the Arctic Ocean (see Paquette and Bourke, 1974;

Table 2
Radiochemical data from the ICEX site

Sample	Depth (m)	^{226}Ra (dpm 100l^{-1})	^{228}Ra (dpm 100l^{-1})	$\frac{^{228}\text{Ra}}{^{226}\text{Ra}}$	^{224}Ra (dpm 100l^{-1})	^{228}Th (dpm 100l^{-1}	^{224}Ra$_{xs}$ (dpm 100l^{-1})
Cast A April 3							
ICEX A-1	10	5.25±0.15	2.02±0.01	0.38±0.01	2.98±0.15	1.19±0.21	1.79±0.26
ICEX A-2	50	5.15±0.07	2.67±0.37	0.52±0.07	1.21±0.17	0.64±0.23	0.57±0.28
ICEX A-3	100	9.31±0.29	4.59±0.54	0.49±0.06	2.91±0.27	1.23±0.30	1.68±0.41
ICEX A-4	150	4.27±0.22	3.44±0.14	0.81±0.05	1.52±0.16	0.43±0.14	1.09±0.21
Cast B April 6							
ICEX B-1	10	4.88±0.13	2.11±0.37	0.43±0.08	1.93±0.24	1.15±0.24	0.78±0.34
ICEX B-2	50	1.60±0.13	1.27±0.06	0.79±0.07	0.70±0.06	0.33±0.11	0.37±0.13
ICEX B-3	102	9.40v0.65	4.64v0.67	0.49±0.08	2.53±0.22	0.79±0.31	1.74±0.38
ICEX B-4	150	9.14±0.61	4.40±0.65	0.48±0.08	2.08±0.20	1.09±0.19	0.99±0.27
ICEX B-5	180	6.99±0.80	4.03±0.24	0.58±0.07	1.56±0.18	1.24±0.20	0.33±0.26
Cast C April 8							
ICEX C-1	10	4.13±0.12	1.62±0.16	0.39±0.04	1.42±0.16	1.19±0.16	0.23±0.23
ICEX C-2	50	8.98±0.12	5.19±0.51	0.58±0.06	2.33±0.17	1.36±0.09	0.97±0.19
ICEX C-3	100	9.17±0.02	4.16±0.15	0.45±0.02	2.27±0.17	1.54±0.24	0.73±0.29
ICEX C-4	150	6.46±0.33	3.62±0.07	0.65±0.04	1.69±0.12	1.52±0.15	0.17±0.19
ICEX C-5	180	9.33±0.10	5.19±0.58	0.56±0.06	1.81±0.17	1.64±0.25	0.17±0.30
Cast D April 10							
ICEX D-1	100	6.84±0.88	3.67±0.14	0.54±0.07	1.80±0.13	1.23±0.09	0.57±0.15
ICEX D-2	210	6.58±0.79	3.39±0.77	0.52±0.13	1.64±0.13	1.30±0.13	0.34±0.18
ICEX D-3	254	6.72±0.71	2.36±0.13	0.35±0.04	1.26±0.13	1.13±0.17	0.13±0.22
ICEX D-4	254	6.15±0.16	1.82±0.85	0.30±0.14	1.16±0.10	1.04±0.14	0.12±0.17

Weingartner et al., 1998; Woodgate et al., 2004). In winter, the canyon flows tend to be strongest when they channel dense, winter-conditioned water off the shelf, and the Alaska Coastal Current is weak and often nonexistent (Weingartner et al., 1998). The tracer-enriched water detected at the 2003 ice camp was of the colder, middle halocline type associated with winter water modification on the shelf. Because of its apparent deep provenance, and because it was detected in early spring, it cannot have originated from the Alaskan Coastal Current. The closest potential source would then appear to be Barrow Canyon, which exits the shelf about 200 km southwest of the ice station site. Herald Canyon is a second possible source, although it is considerably farther from the ice station site (~400 km) and lies more nearly westward.

Down-canyon current speeds in Barrow Canyon have been observed well in excess of 30 cm s^{-1} (Weingartner et al., 1998; Pickart et al., 2004), the speed required to advect the ^{224}Ra-rich water from the canyon mouth to the ice-camp site over the requisite brief interval. However, dynamics associated with such density flows dictate that these waters turn to the right under the influence of rotation and flow along isobaths (Chapman and Gawarkiewicz, 1995). Pickart et al. (2005) present a field-based analysis of the dynamics controlling northward-flowing winter-modified water where it exits Barrow Canyon and extend their results, by implication, west to Herald Canyon. They argue that the dense current issuing from the canyon mouths on the upper continental slope is dynamically unstable, breaking down into meanders and eddies. They further purport that the resulting eddies move offshore and contribute significantly to the admixture of Pacific origin water that conditions upper ocean waters in the Canada Basin. Such eddies can have diameters of 20–30 km, and tangential current speeds of 20–30 cm s^{-1} (e.g. Manley and Hunkins, 1985). However, analyses by Muench et al. (2000) of an eddy found in 1998 near the location of the ice-camp site suggest an offshore transit speed of only a few cm s^{-1}, clearly inadequate to move the tracer-enriched water from the shelf break to the ice camp within the short lifetime of the tracer. There are few detailed field

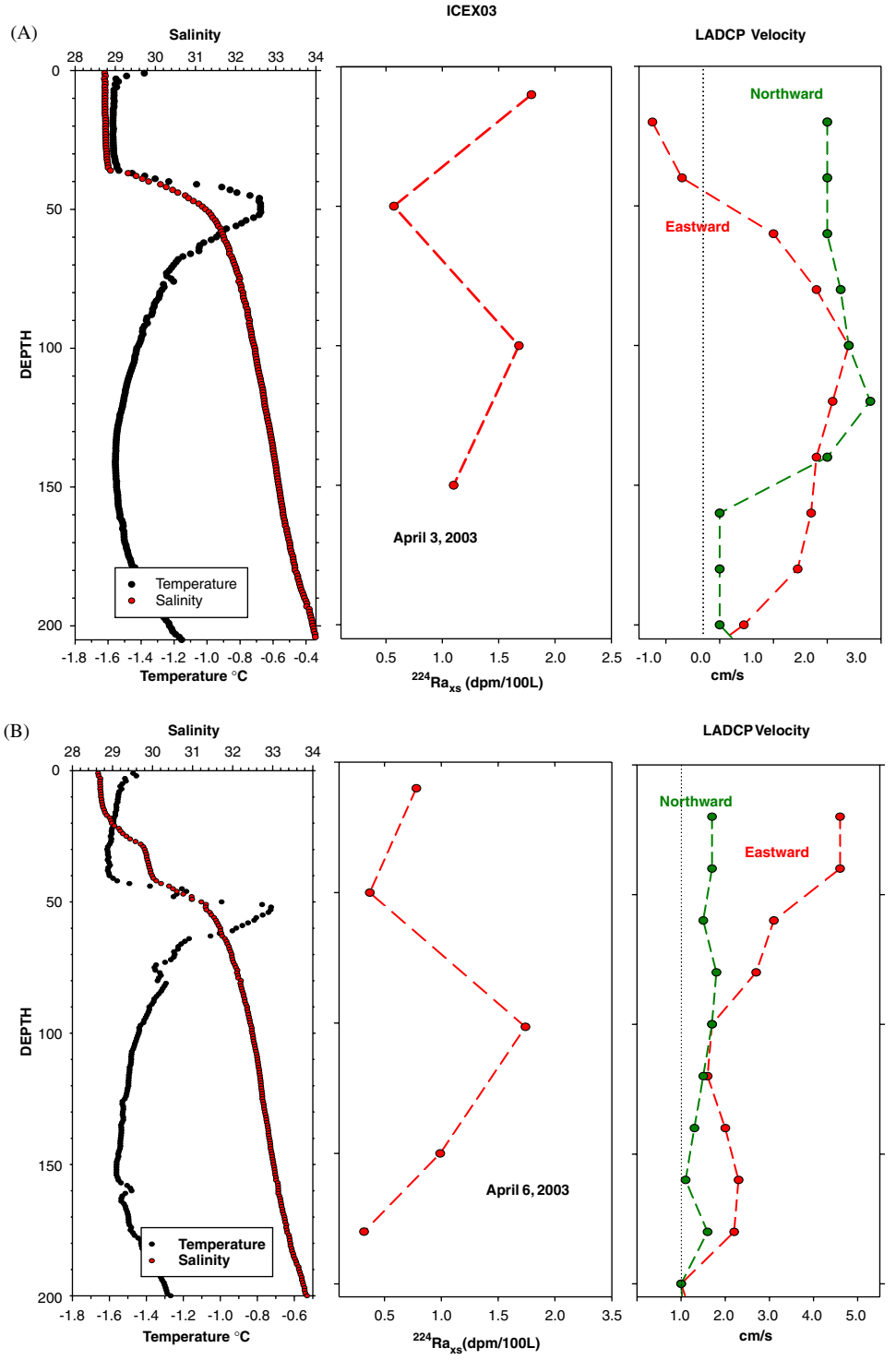

Fig. 6. (A–D). Depth profiles of several properties for ICEX03 (April 3, 6, 8, 10) Left panel: temperature and salinity. Middle panel: $^{224}Ra_{xs}$. Right panel: the northward and eastward LADCP speeds.

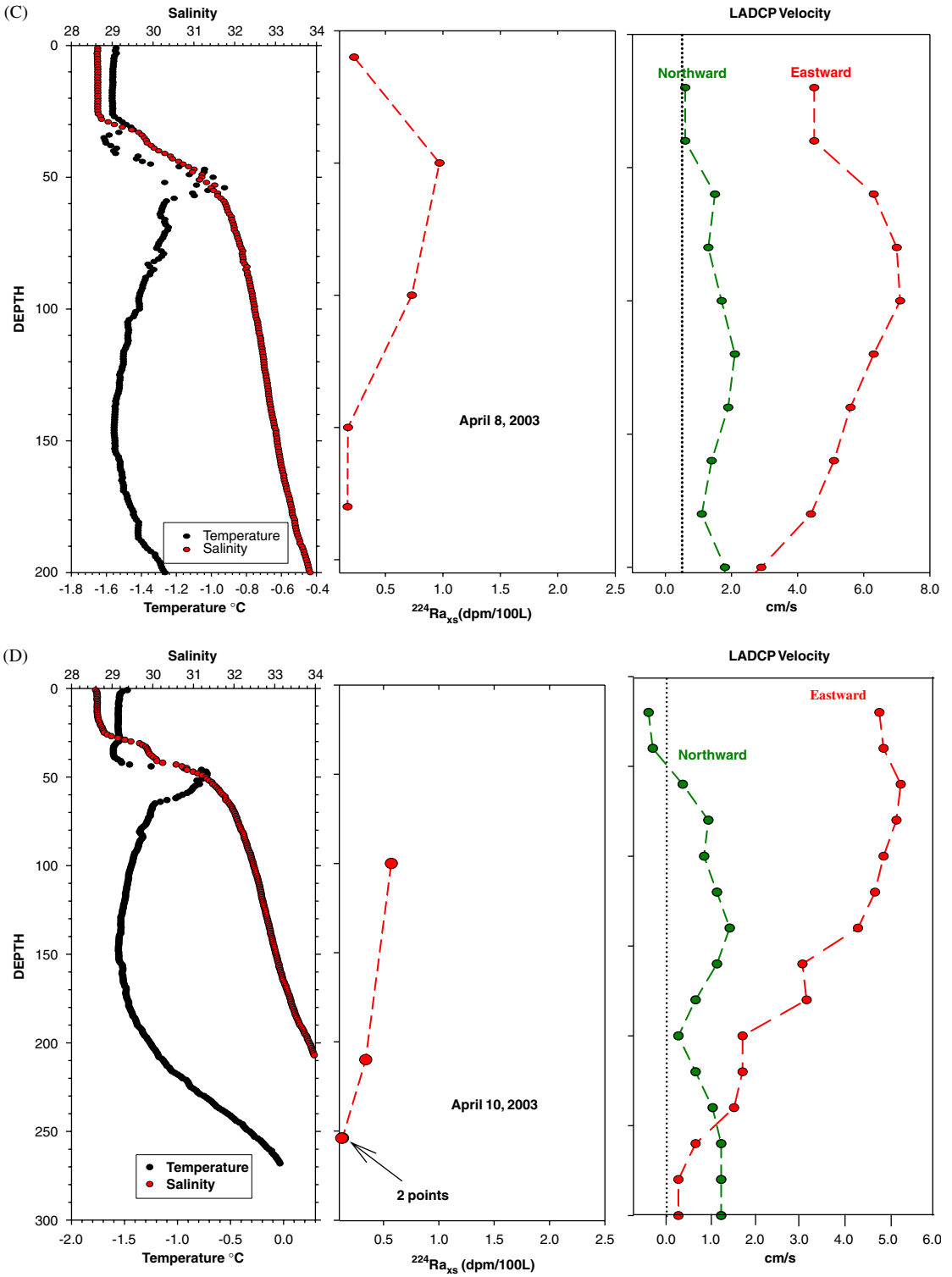

Fig. 6. (*Continued*)

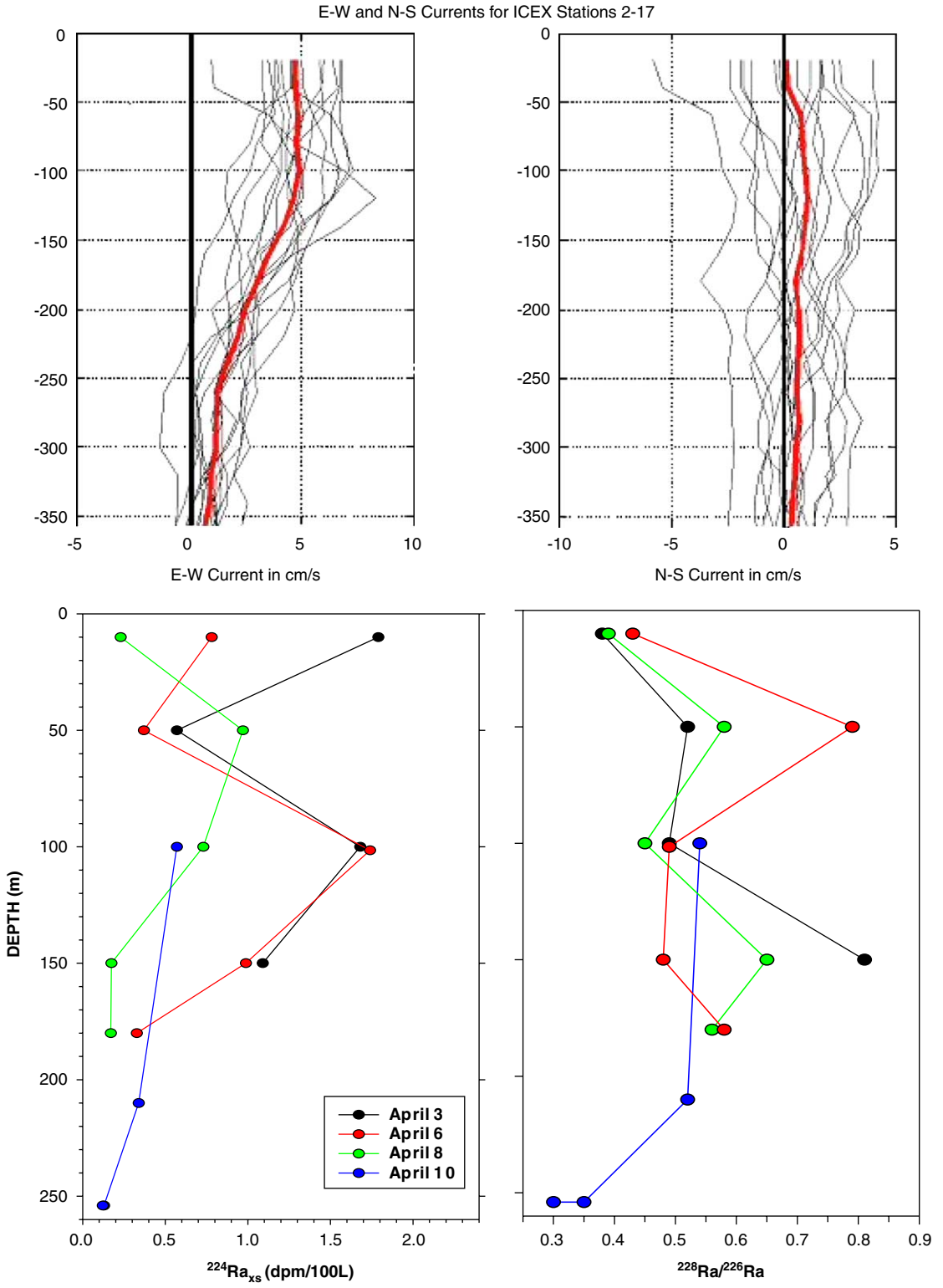

Fig. 7. Top left: east–west currents (cm s^{-1}) for all ICEX stations, 3–12 April 2003. Top right: north–south currents (cm s^{-1}) for all ICEX stations, 3–12 April 2003. The red lines indicate averages over the study period. Bottom left: $^{224}Ra_{xs}$ profiles for ICEX 2003. Bottom right: $^{228}Ra/^{226}Ra$ profiles for ICEX 2003.

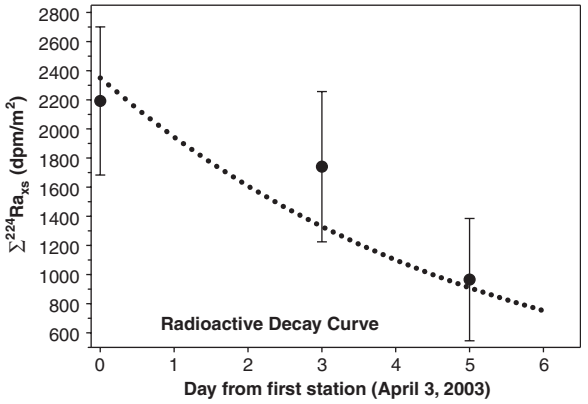

Fig. 8. Plot showing the rate of decrease in integrated $^{224}Ra_{xs}$ measured at the ICEX station (solid circles) as compared with the theoretical decay rate (dotted line).

observations of Canada Basin eddies, and none have been tracked from a source region into the basin other than indirectly by use of tracers.

If the ^{224}Ra-rich Pacific water observed at the ice camp was originally present in an eddy off Barrow Canyon, then we can examine some hypothetical scenarios. It seems unlikely that eddy generation and migration alone can account for our observations. Assume development of an eddy off Barrow Canyon having a diameter of 40 km, which is large but not impossible, and a tangential speed of $>30\,cm\,s^{-1}$, which is also physically possible given that both down-canyon and shelf break current flow events have been observed to exceed this speed. Assume also that the eddy breaks loose from a meander well seaward of the shelf break. Conceptually, then, we might already have the desired water within 100 km or less of the ice-camp site. We would still need, though, to maintain a very high offshore speed in order to attain the ice camp site within the timescale dictated by the ^{224}Ra decay time. Such a strong eddy migration speed is unlikely given frictional decay from the overlying pack-ice cover, and is inconsistent with the $1–2\,cm\,s^{-1}$ migration rates deduced by Muench et al. (2000). Alternately, suppose that a very large meander, with amplitude approaching 200 km, develops in the shelf break current. A meander of this size would also be expected to have large associated current speeds, and the relatively weak northeastward currents observed at the ice camp might have represented the decayed remnant of such a highly energetic eddy or meander. This is consistent with the decay of the integrated $^{224}Ra_{xs}$ measured over our observational period (Fig. 8). Such meanders can occur in association with major currents such as the Gulf Stream although they seem less likely in the much lower energy and highly bathymetrically controlled regime along the upper slope north of Alaska. Ongoing analyses of physical oceanographic data collected from the shelf break region during winter 2003 are expected to greatly improve our understanding of the regional shelf break dynamics and the possible implications for northward transport.

Finally, energetic wind forcing can contribute to rapid northward transport of water from the shelf break, which may be relevant in this case. Strong easterly (upwelling favorable) winds occurred in the shelf break region about a week prior to the ICEX observations, associated with the appearance of cold halocline water offshore (R. Pickart, pers. comm.). Rapid northward motion of sea ice also was noted at about the same time in the region just seaward of the shelf break (J. Haarpaintner, pers. comm.), and this may have reflected an underlying northward flow. Remnants of a vigorous offshore wind-forced flow may have persisted in the upper halocline, where it would have met with decreased frictional resistance because of the strong vertical stratification, allowing it to reach the ICEX site in a short time frame. Rigorous investigation of such a possibility lies, however, outside the scope of this paper.

5. Conclusions

We applied ^{228}Ra/^{226}Ra and $^{224}Ra_{xs}$ measurements to investigate exchange between the Arctic shelves and interior in the western Arctic. Results from the SBI 2002 program suggest that water-column properties over the Chukchi Shelf are transported slowly across the shelf-break. The observation of $^{224}Ra_{xs}$ approximately 200 km offshore at the ICEX03 site was surprising and raises questions as to a physical mechanism capable of transporting shelf properties to the interior so quickly. Possibilities include mesoscale features associated with the shelf break currents or wind-forced events that rapidly carry shelf properties into the basin interior. If common, such features would have significant implications for the transport to deeper basin waters of short-lived chemical and still-viable biological species typically found only on the inner shelf.

Acknowledgements

This work was supported by National Science Foundation Polar Programs Grant OPP 0124872 and ONR Grant N000140210652 to the University of Miami (DK) and ONR Grant N00014-03-1-0067 to Earth and Space Research (RDM). We extend thanks to Drs. Robert Pickart, Tom Weingartner and Dennis Hansell for very valuable comments and discussion, Dr. M. Stephens for field and laboratory assistance, Dr. Lee Cooper for providing the oxygen isotope analyses, Dr. Joerg Haarpaintner for providing sea ice motions in the vicinity of the ICEX station, and the crew of the research ice-breaker USCGC HEALY for their capable and enthusiastic field support. This is Earth and Space Research Contribution No. 036.

References

Aagaard, K., Coachman, L.K., Carmack, E.C., 1981. On the halocline of the Arctic Ocean. Deep-Sea Research 28, 529–545.

Anderson, L.G., 1995. Chemical oceanography of the Arctic and its shelf seas. In: Smith, Jr., W.O., Grebmeir, J.M. (Eds.), Arctic Oceanography: Marginal Ice Zones and Continental Shelves, Coastal and Estuarine Studies 49. American Geophysical Union, Washington, DC, pp. 183–202.

Anderson, L.G., 2002. DOC in the Arctic Ocean. In: Hansell, A.A., Carlson, C.A. (Eds.), Biogeochemistry of Marine Dissolved Organic Matter. Academic Press, San Diego, pp. 665–683.

Arctic Monitoring and Assessment Programme (AMAP), 1997. The AMAP International Symposium on Environmental Pollution in the Arctic, Tromso, Norway, June 1–5, 1997, extended abstracts, vol. 1, 432pp.

Chapman, D.C., 2000. The influence of an alongshelf current on the formation and offshore transport of dense water from a coastal polynya. Journal of Geophysical Research 105, 24007–24019.

Chapman, D.C., Gawarkiewicz, G.G., 1995. Offshore transport of dense shelf water in the presence of a submarine canyon. Journal of Geophysical Research 100, 13373–13387.

Coale, K.H., Bruland, K.W., 1985. ^{234}Th: ^{238}U disequilibria within the California current. Limnology and Oceangraphy 30 (1), 22–33.

Cooper, L.W., Whitledge, T.E., Grebmeier, J.M., Weingartner, T., 1997. The nutrient, salinity and stable oxygen isotope composition of Bering Sea and Chukchi Sea water in and near the Bering Strait. Journal of Geophysical Research 102, 12563–12573.

D'Asaro, E.A., 1988a. Observations of small eddies in the Beaufort Sea. Journal of Geophysical Research 93, 6669–6684.

D'Asaro, E.A., 1988b. Generation of submesoscale vortices: a new mechanism. Journal of Geophysical Research 93, 6685–6693.

Gawarkiewicz, G.G., 2000. Effects of ambient stratification and shelfbreak topography on offshore transport of dense water on continental shelves. Journal of Geophysical Research 105, 3307–3324.

Gawarkiewicz, G.G., Chapman, D.C., 1995. A numerical study of dense water formation and transport on shallow, sloping continental shelves. Journal of Geophysical Research 100, 4489–4507.

Hansell, D.A., Kadko, D., Bates, N.R., 2004. Non-conservative behavior of terrigenous dissolved organic carbon in the Western Arctic Ocean. Science 304, 858–861.

Kaufman, A., Trier, R.M., Broecker, W.S., Feely, H.W., 1973. Distribution of ^{228}Ra in the world ocean. Journal of Geophysical Research 78, 8827–8847.

Kaufman, A., Li, Y-H., Turekian, K.K., 1981. The removal rates of ^{224}Th and ^{228}Th from waters of the New York Bight. Earth and Planetary Science Letters 54, 385–392.

Manley, T.O., Hunkins, K., 1985. Mesoscale eddies of the Arctic Ocean. Journal of Geophysical Research 90, 4911–4930.

Macdonald, R.W., Carmack, E.C., McLaughlin, F.A., Kalkner, K.K., Swift, J.H., 1999. Connections among ice, runoff and atmospheric forcing in the Beaufort Gyre. Geophysical Research Letters 26, 2223–2226.

McLaughlin, F.A., Carmack, E.C., Macdonald, R.W., Melling, H., Swift, J.H., Wheeler, P.A., Sherr, B.F., Sherr, E.B., 2004. The joint roles of Pacific and Atlantic-origin waters in the Canada Basin, 1997–1998. Deep-Sea Research I 51, 107–128.

Melling, H., Moore, R.M., 1995. Modification of halocline water source waters during freezing on the Beaufort Sea shelf: evidence from oxygen isotopes and dissolved nutrients. Continental Shelf Research 15, 81–113.

Michel, J., Moore, W.S., King, P.T., 1981. γ-Ray spectrometry for determination of radium-228 and radium-226 in natural waters. Analytical Chemistry 53, 1885–1889.

Moore, W.S., Arnold, R., 1996. Measurement of ^{223}Ra and ^{224}Ra in coastal waters using a delayed coincidence counter. Journal of Geophysical Research 101, 1321–1329.

Moore, W.S., Key, R.M., Sarmiento, J.L., 1985. Techniques for precise mapping of ^{226}Ra and ^{228}Ra in the ocean. Journal of Geophysical Research 90, 6983–6994.

Muench, R.D., Gunn, J.T., Whitledge, T.E., Schlosser, P., Smethie Jr., W.S., 2000. An Arctic Ocean cold core eddy. Journal of Geophysical Research 105, 23997–24006.

Paquette, R.G., Bourke, R.H., 1974. Observations on the coastal current of Arctic Alaska. Journal of Marine Research 32, 195–207.

Pickart, R.S., Weingartner, T.J., Pratt, L.J., Zimmermann, S., Torres, D.J., 2005. Flow of winter-transformed Pacific water into the western Arctic. Deep-Sea Research II, this issue [doi:10.1016/j.dsr2.2005.10.009].

Reimnitz, E., Barmes, P.W., Weber, W.S., 1993. Particulate matter in pack ice of the Beaufort Gyre. Journal of Glaciology 39, 186–193.

Rutgers van der Loeff, M.M., Key, R.M., Scholten, J., Bauch, D., Michel, A., 1995. ^{228}Ra as a tracer for shelf water in the Arctic Ocean. Deep-Sea Research II 42, 1533–1553.

Rutgers van der Loeff, M., Kuhne, S., Wahsner, M., Holtzen, H., Frank, M., Ekwurzel, B., Mensch, M., Rachold, V., 2003. ^{228}Ra and ^{226}Ra in the Kara and Laptev seas. Continental Shelf Research 23, 113–124.

Sambrotto, R., 1996. Transfer of shelf derived carbon to the interior of the Arctic Ocean. In: Tucker, W., Cate, D. (Eds.),

The 1994 Arctic Ocean Section: The First Major Scientific Crossing of the Arctic Ocean. US Army Cold Region Research and Engineering Laboratory, Hanover, NH, USA.

Schauer, U., Muench, R.D., Rudels, B., Timokhov, L., 1997. Impact of eastern Arctic shelf waters on the Nansen Basin intermediate layers. Journal of Geophysical Research 102, 3371–3382.

Smith, J.N., Moran, S.B., Macdonald, R.W., 2003. Shelf–basin interactions in the Arctic Ocean based on ^{210}Pb and Ra isotope tracer distributions. Deep-Sea Research I 50, 397–416.

Wallace, D., Moore, W., Jones, R.M., 1987. Ventilation of the Arctic Ocean cold halocline: rates of diapycnal and isopycnal transport, oxygen utilization and primary production inferred using chlorofluoromethane distributions. Deep-Sea Research 34, 1957–1979.

Walsh, J.J., McRoy, C.P., Coachman, L.K., Goering, J.J., Nihoul, J., Whitledge, T.E., Blackburn, T.H., Parker, P.L., Wirick, C.D., Shuert, P.G., Grebmeier, J.M., Springer, A.M., Tripp, R.B., Hansell, D.A., Djenidi, S., Deleersnijder, E., Henriksen, K., Lund, B.A., Andersen, P., Muller-Karger, F.E., Dean, K.K., 1989. Carbon and nitrogen cycling within the Bering/Chukchi Seas: source regions for organic matter effecting AOU demands of the Arctic Ocean. Progress in Oceanography 22, 277–359.

Walsh, J.J., Dieterle, D.A., Muller-Karger, F.E., Aagaard, K., Roach, A.T., Whitledge, T.E., Stockwell, D., 1997. CO_2 cycling in the coastal ocean. II. Seasonal organic loading to the Canadian Basin from source waters south of the Bering Strait. Continental Shelf Research 17, 1–36.

Weingartner, T.J., Cavalieri, D.J., Aagaard, K., Sasaki, Y., 1998. Circulation, dense water formation, and outflow on the northeast Chukchi shelf. Journal of Geophysical Research 103, 7647–7661.

Winsor, P., Chapman, D.C., 2004. Pathways of Pacific water across the Chukchi Sea: a numerical model study. Journal of Geophysical Research 109, C03002.

Woodgate, R.A., Aagaard, K., Weingartner, T.J., 2004. A year in the physical oceanography of the Chukchi Sea: moored measurements from autumn 1990–1991. Deep-Sea Research II, this issue [doi:10.1016/j.dsr2.2005.10.016].